Functional Analysis of SARS-CoV-2 Proteins in Drosophila Identifies Orf6-induced Pathogenicity Attenuated by Selinexor

Jun-yi Zhu
University of Maryland School of Medicine
Jin-Gu Lee
University of Maryland School of Medicine
Joyce van de Leemput
University of Maryland School of Medicine
Hangnoh Lee
University of Maryland School of Medicine
Zhe Han (ZHan@som.umaryland.edu)
Center for Precision Disease Modeling, Department of Medicine, University of Maryland School of Medicine, Baltimore, Maryland https://orcid.org/0000-0002-5177-7798

Research

Keywords: bioinformatic analysis, COVID-19, SARS-CoV2 genes, Selinexor

Posted Date: January 11th, 2021

DOI: https://doi.org/10.21203/rs.3.rs-141269/v1

Version of Record: A version of this preprint was published on March 25th, 2021. See the published version at https://doi.org/10.1186/s13578-021-00567-8.

Abstract

Background: SARS-CoV-2 causes COVID-19 with a widely diverse disease profile that affect many different tissues. The mechanisms underlying its pathogenicity in host organisms remain unclear. Animal models for study the pathogenicity of SARS-CoV-2 proteins are lacking.

Methods: Using bioinformatic analysis, we showed that the majority of the virus-host interacting proteins are conserved in *Drosophila*. Therefore, we generated a series of transgenic lines for individual SARS-CoV-2 genes and used the Gal4-UAS system to express them in various tissues to study their pathogenicity.

Results: We found that the Nsp6, Orf6 and Orf7a transgenic flies displayed reduced trachea branching and muscle deficits resulting in “held-up” wing phenotype and poor climbing ability. Furthermore, muscle tissue in these flies showed dramatically reduced mitochondria. Since Orf6 was found to bind nucleopore proteins XPO1, we tested Selinexor, a drug that inhibits XPO1, and found that it could attenuated the Orf6-induced lethality and tissue-specific phenotypes in flies.

Conclusions: Our studies here established new *Drosophila* models for studying the function of SARS-CoV2 genes, identified Orf6 as a highly pathogenic protein in various tissues, and demonstrated the effects of Selinexor for inhibiting Orf6 toxicity with an *in vivo* model system.

Introduction

SARS-CoV-2 (severe acute respiratory syndrome coronavirus 2), the cause of coronavirus disease 2019 (COVID-19), is the latest in a string of outbreaks in the human population caused by highly pathogenic coronaviruses. Its high transmission rate and virulence have culminated in a pandemic to which no end is insight at the time of this writing. At the time of this writing, SARS-CoV-2 has infected nearly 80 million people globally, causing more than 1,7 million deaths (source: Johns Hopkins University). While SARS-CoV-2 shares many similarities with its predecessors, SARS-CoV (2002-2004) and MERS-CoV (Middle East respiratory syndrome-CoV; 2012), investigations have already revealed several unique features. For example, the SARS-CoV-2 spike (S) protein structure includes a distinct loop with flexible glycyl residues in place of the SARS-CoV rigid prolyl residues. Molecular modeling has indicated the SARS-CoV-2 receptor binding domain has a higher affinity for ACE2 compared to its SARS-CoV counterpart (Y. Chen, Guo, Pan, & Zhao, 2020), which might contribute to its high virulence. These findings highlight the important roles specific viral genes can play, yet very little is known of the functions of individual SARS-CoV-2 proteins and the host systems they affect.

The SARS-CoV-2 genome encodes 28 confirmed proteins (Figure 1A). These include the polyproteins Orf1ab and Orf1a that are further cleaved into 165 non-structural proteins (Nsp1-16) that form the viral transcription/replication complex, as well as the 4 structural proteins (spike (S), envelope (E), membrane (M) and nucleocapsid (N) proteins) and 8 accessory proteins (Orf3a, Orf3b, Orf6, Orf7b, Orf8, Orf9b and Orf 10) (Gordon et al., 2020; Yoshimoto, 2020). The functional significance of these accessory proteins remains largely unresolved, since they lack well-defined domain structures. Interestingly, they are also the

least conserved between the SARS-CoV-2 and SARS-CoV viruses (Gordon et al., 2020). In fact, specific host interaction networks have been shown for each of the SARS-CoV-2 proteins (Gordon et al., 2020). In order to identify targets and develop effective therapeutics for COVID-19, it will be vital to understand how SARS-CoV-2 hijacks host pathways and which of its proteins are key for these interactions and ultimately are the primary determinants of pathogenicity.

Human models are limited to in vitro studies which lack a whole body context, while conventional animal models are not conducive to screening multiple individual proteins and many, including mice, have been hampered by lacking natural susceptibility to SARS-CoV-2 infection (Takayama, 2020). Therefore, we sought to establish a new animal model, namely the fruit fly (*Drosophila*). Notably, we found that the vast majority of the human host protein interactome identified for SARS-CoV-2 proteins have fly orthologs, and their related biological processes are conserved in flies (Figure 1B and C; Supplemental Table S1). *Drosophila*'s ease-of-use, while offering complexity with all major organs present (including heart, lung, kidney, muscle, blood and brain) and encoded by a compact genome with little redundancy, combined with the abundance of available genetic resources, has already been effectively applied to investigate several human relevant viruses in recent years (Hughes et al., 2012), including HIV-1 and Zika. For example, the HIV-1 *Nef* gene was studied in *Drosophila* using the *UAS-Gal4* system (Lee, Park, Jung, & Chung, 2005). The study discovered the interaction between the HIV-1 Nef protein and the JNK and NF-kappaB signaling at the plasma membrane of fly wing disc cells, both are evolutionary highly conserved signaling pathways. The HIV-1 Tat protein was similarly studied in flies and found to disrupt microtubule polymerization and kinetochore dynamics via a direct interaction with tubulin (Battaglia, Zito, Macchini, & Gigliani, 2001). This finding led to the discovery of interaction between Tat and human tubulin proteins and the important role of Tat in inducing apoptosis of human cells through targeting the microtubule network in human 293T cells (D. Chen, Wang, Zhou, & Zhou, 2002). *Drosophila* studies, using the *UAS-Gal4* system to express Zika virus (ZIKV) proteins in specific tissues, have also provided significant contributions in the study of ZIKV infection and related microcephaly. One such study found that neurons employ NF-kappaB-dependent inflammatory signaling in response to ZIKV infection (Liu et al., 2018). This, in turn, induces expression of *Drosophila* stimulator of interferon genes (dSTING) specifically in the brain of ZIKV infected flies. Activation of dSTING leads to antiviral autophagy as an innate defense to control the viral infection thereby restricting ZIKV to the brain. Another high-profile study used fly models to demonstrate that genetic variants in ANKLE2, a protein linked to hereditary microcephaly, and ZIKV protein NS4A which interacts with and inhibits Ankle2 protein function, converge on the same pathological pathways (Link et al., 2019). They elegantly demonstrate that Ankle2 interaction with Ballchem/VRK1 regulates asymmetric protein localization during neuroblast division, and that disruption of this pathway leads to microcephaly in both human patients due to genetic causes and flies induced by ZIKV infection. Further, a study into host transcriptomics changes following ZIKV infection in *Drosophila* adult flies, revealed the importance of the JAK/STAT signaling pathway in viral pathogenesis (Harsh, Fu, Kenney, Han, & Eleftherianos, 2020). Interestingly, further exploration of the interaction between JAK/STAT signaling and the individual ZIKV non-structural proteins revealed tissue-specific regulation of viral infection via highly conserved host signaling pathways. Together, these studies demonstrate that

flies provide a powerful model to identify the prime mechanistic tissue-specific pathways used by specific viral pathogenic proteins, and that these pathways are conserved from fly to human. However, as of yet, no literature reports the use of *Drosophila* to study SARS-CoV-2.

We used *Drosophila* to identify the foremost pathogenic SARS-CoV-2 genes, and then examined their effects on host function in a whole organism. Data revealed SARS-CoV-2 Orf6, Orf7a and Nsp6 proteins display pathogenicity *in vivo*. Each of these proteins individually can cause developmental lethality, reduced lifespan, defect in trachea morphology (reduced branching in fly equivalent of lung), aberrant muscle function without significant morphological changes, and reduced mitochondria in muscle tissue. Interestingly, while all three proteins induced similar phenotypic defects, their underlying pathomechanism appears to be different. Selinexor, an FDA-approved selective inhibitor of nuclear export and predicted to disrupt SARS-CoV-2 Orf6 interaction with the host nuclear pore system, was able to counteract virus protein induced developmental lethality in Orf6 transgenic flies, but not in flies with Orf7a or Nsp6 overexpression. Indeed, Selinexor attenuated each of the observed phenotypes in SARS-CoV-2 Orf6 transgenic flies. Taken together, these data demonstrate *Drosophila* provides a valuable resource for studying SARS-CoV-2 mechanism-of-action and pharmacological interventions. Furthermore, these findings make a strong case for the importance of studying individual SARS-CoV-2 proteins and illustrate their potential as therapeutic targets to counteract the pathogenic mechanisms culminating in COVID-19 symptomatology, as a complement to viral inhibition.

Results

SARS-CoV-2 Nsp6, Orf6 and Orf7a transgene expression causes developmental lethality and reduced longevity in flies

The SARS-CoV-2 genome encodes 28 confirmed proteins (Orf9c genetic code does not lie within the verified SARS-CoV-2 open reading frame) (Figure 1A). To date, few studies have looked at the individual viral proteins, those that did have been limited to *in vitro* models. Here we use the fruit fly, *Drosophila melanogaster*, as a whole organism model to carry out a detailed study of pathogenic effect and function of individual SARS-CoV-2 proteins. We integrated data on predicted topology and subcellular localization (based on topological motifs such as transmembrane domain, signal peptide, membrane-embedded alpha-helix and nuclear localization sequence), with data from UniProt Knowledgebase (UniProt, 2019) and the scientific literature to prioritize viral genes based on likelihood to instigate pathogenic host interactions. Viral proteins with main purported functions in viral entry, replication or packaging were initially not favored as they remain a focus of much of the latest literature. Twelve SARS-CoV-2 proteins (Nsp1, Nsp2, Nsp3, Nsp6, Orf3a, Orf3b, Orf6, Orf7a, Orf7b, Orf8, Orf9b and Orf10) were thus prioritized for analysis. In order to investigate the function of SARS-CoV-2 genes *in vivo*, we produced transgenic *Drosophila* lines carrying each of these individual SARS-CoV-2 genes, in the *UAS-Gal4*^{Tub} system. The ubiquitous enhancer Tubulin (Tub) is active in all tissues and throughout development from embryonic stages, therefore we reasoned that Tub enhancer driven expression of SARS-CoV-2 genes that are primary determinants of virus pathogenicity would result in lethality.

For this assay, male and female flies of the designated genotypes were crossed to produce progeny carrying the *UAS-SARS-CoV-2 gene* construct, with ubiquitous expression of the individual virus gene driven by *Tub-Gal4* (red eyes, long hair), or the balancer (orange eyes, short hair) (Figure 2A). Ratios of these two variants among the progeny showed high mortality among flies expressing SARS-CoV-2 Nsp6, Orf6 or Orf7a, and a moderate increase in mortality among Nsp3 transgenic flies (Figure 2B and C). In addition, we monitored fly survival rates. Under typical maintenance conditions, the majority of wild type flies survive 50-60 days. Orf6 and Orf7a expression flies displayed reduced lifespan such that all flies had died by 20 and 18 days, respectively (Figure 2D). Nsp6 expression was associated with a severe lifespan reduction such that flies survived 12 days at most (Figure 2D). Nsp3 which induced more moderate developmental lethality, also considerably reduced fly lifespan to 26 days. Interestingly, though Orf3a expression did not cause developmental lethality in our mortality index, it did shorten adult fly lifespan (34 days maximum), which suggests it may induce more moderate levels of toxicity or affect adult fly pathways. Together, these results suggest that Nsp6, Orf6 and Orf7a might be primary determinants of SARS-CoV-2 pathogenicity.

SARS-CoV-2 Nsp6, Orf6 and Orf7a transgene expression leads to reduced branching of *Drosophila* trachea

COVID-19 is an acute respiratory disease which is characterized by pneumonia when disease progresses, as well as additional complications. Due to its primary effect on the lungs, we tested whether expression of SARS-CoV-2 Nsp6, Orf6 and Orf7a—most pathogenic viral proteins based on our developmental lethality and survival assays—by themselves would lead to change in long morphology. The *Drosophila* tracheal system is similar to human lung and shares a striking resemblance in branching morphology (Figure 3A). In wild type *Drosophila* larvae, the tracheal system contains a central branch and multiple classes of terminal branches (Figure 3B). SARS-CoV-2 Nsp6, Orf6 and Orf7a expression led to dramatically reduced numbers of class II terminal branches, while the central branch and class I terminal branches appeared unchanged (Figure 3C and D). The changed morphology could result in a functional defect of the fly tracheal system and possibly contribute to the reduced developmental viability we observed in these flies.

SARS-CoV-2 Nsp6, Orf6 and Orf7a transgene expression results in dysfunctional muscle and reduced presence of mitochondria

We examined whether Nsp6, Orf6 and Orf7a expression affected fly locomotion ability. A climbing assay revealed locomotion defects in SARS-CoV-2 Nsp6, Orf6 and Orf7a transgenic flies (Figure 4A). Interestingly, we observed flies with an “held-up” wing position phenotype among those expressing SARS-CoV-2 Nsp6, Orf6 or Orf7a (Figure 4B and C). The “held-up” wing defect is typically due to a defect of the indirect flight muscle. Hence, we took a closer look at the indirect flight muscle morphology in the Nsp6, Orf6 and Orf7a transgenic flies, but did not observe any significant morphological changes in muscle fiber (Figure 4D). However, when studying the mitochondria in the indirect flight muscle of these flies, their numbers were dramatically reduced (Figure 4D and E). Mitochondria are essential for muscle function

and their significant reduction could explain both the “held-up” wing phenotype and the reduced climbing ability of the adult flies. These data suggested SARS-CoV-2 Nsp6, Orf6 and Orf7a may affect muscle function by reducing the available function mitochondria. Additional studies are needed to understand the full mechanism underlying these findings, and their implications.

Selinexor attenuates SARS-CoV-2 Orf6 induced developmental lethality, aberrant tracheal branching, locomotion defect and reduced mitochondria

Selinexor, an FDA-approved selective inhibitor of nuclear export (Kashyap et al., 2016), has been proposed as potential treatment for COVID-19, based on its predicted ability to disrupt SARS-CoV-2 Orf6 interaction with the mRNA nuclear export complex (RAE1 and NUP98) (Gordon et al., 2020). These Orf6 interaction proteins are conserved between human and fly (Figure 5A). Therefore, we tested whether Selinexor could rescue the various phenotypes observed in our SARS-CoV-2 Orf6 overexpression flies. The flies were treated with different Selinexor doses (0, 0.1 μM, 0.2 μM and 0.5 μM) from larval stage. We found 0.2 μM, but not 0.1 μM, Selinexor treatment attenuated the developmental lethality caused by Orf6, but not the lethality observed in Nsp6 or Orf7a transgenic flies (Figure 5B). At 0.5 μM, the highest dose tested, Selinexor was toxic to the flies and caused complete lethality in the Orf6 transgenic and wild type (w^{1118}) flies (data not shown). Further, show 0.2 μM Selinexor treatment in the flies significantly attenuated SARS-CoV-2 Orf6 induced reduction in tracheal branching (Figure 5C and D), as well as the locomotion defect, “held-up” wing phenotype and mitochondrial loss observed in the indirect flight muscle (Figure 6 A-D). Together these findings indicate the Selinexor, and possibly other nuclear transport inhibitors, might provide an effective targeted treatment strategy for SARS-CoV-2 Orf6 protein induced cellular damage through blocking viral interaction with the host nuclear pore complex.

Discussion

SARS-CoV-2, like most viruses, relies heavily on host functions to complete its life cycle. It encodes structural proteins (S, E, M and N) that provide a capsule structure for the virion, non-structural proteins (Nsp1-16) that interact with and modify host protein systems for virus transcription and replication, and accessory proteins (Orfs). The latter appear more variable across viruses, even within the same genus, and their functions are less understood; some are required for replication, while others are engaged in transforming the host environment to be more conductive of virus replication and spread. For example, by evading or counteracting the host immune response. Given their highly specialized functions and host interactions, it seems reasonable to assume some viral proteins are more pathogenic than others. Indeed, this has been shown for HIV-1 (Fraser et al., 2014), ZIKV (Wang, Thurmond, Islas, Hui, & Hai, 2017), SARS-CoV (Khan et al., 2006; Kopecky-Bromberg, Martinez-Sobrido, & Palese, 2006; Law et al., 2005; Schaecher, Touchette, Schriewer, Buller, & Pekosz, 2007; Yuan, Shan, Zhao, Chen, & Cong, 2005) and for SARS-CoV-2 (Lee et al., this issue). Toxicity in an *in vitro* system does not capture the complexity of pathogenicity in a whole organism, nor does it provide any indication as to what tissues might be most infected. To answer these questions, we looked at the fly. Animal studies for SARS-CoV-2 have been limited (Bao et al., 2020; Dinnon et al., 2020; Hassan et al., 2020; Israelow et al., 2020; Rockx et al., 2020; Yu et al., 2020), and none

have looked at individual proteins. The *Drosophila* system is well-established and has been instrumental in identifying some of the primary detrimental virus proteins and their interaction with host pathways in HIV-1 and ZIKV infections (Battaglia et al., 2001; Harsh et al., 2020; Hughes et al., 2012; Lee et al., 2005; Link et al., 2019; Liu et al., 2018).

Encouraged by the considerable conservation of the SARS-CoV-2 virus-host interaction network proteins between human and fly (Figure 1), we tested toxicity of individual viral proteins in fly. Transgenic fly lines expressed each of the SARS-CoV-2 genes predicted to be most likely pathogenic based on available resources. SARS-CoV-2 Orf6, Nsp6 and Orf7a proofed most pathogenic based on mortality at eclosion (*i.e.* prior to adult fly emerges) and longevity (Figure 2), these were also most toxic in our human *in vitro* screen using HEK 293T (Lee et al., this issue). Nsp3 expression in fly also caused developmental lethality and reduced longevity, albeit with smaller effect than the main pathogenic proteins. Notably, Nsp3 was not found to affect viability of the human cells (Lee et al., this issue). This does not exclude possible toxicity to cellular pathways that do not directly affect apoptosis and reflects the added value of looking in a live animal model which captures effects on all cell types and tissues. Orf3a, on the other hand, displayed no detectable change in developmental mortality, however it significantly reduced fly lifespan and showed cytotoxicity in HEK 293T (Lee et al., this issue). These data suggest that in fly, Orf3a either induced relatively moderate toxicity or interacts with, and affects, host systems that play a role after adult hatching. Taken together, these findings show the fly system can accurately capture SARS-CoV-2 individual protein pathogenicity.

Similar to host tissue-specific effects based on tissue differences in proteins and pathways, the individual virus proteins are equally important in determining the effects on a tissue. Our data revealed similar phenotypic read-outs for SARS-CoV-2 Orf6, Nsp6 and Orf7a expression across the various tissues in fly, however, the underlying pathomechanisms are likely different. Based on available literature for SARS-CoV-2 and related SARS-CoV proteins, we can make some predictions as to the pathways affected by each. Orf6 has been known to have interferon (IFN) antagonistic properties based on previous coronaviruses. This function has been retained by SARS-CoV-2 Orf6 (J. Y. Li et al., 2020), with comparable ability as its SARS-CoV equivalent to interfere with interferon production (Yuen et al., 2020). SARS-CoV Orf6 has been shown to inhibit primary interferon production (Kopecky-Bromberg, Martinez-Sobrido, Frieman, Baric, & Palese, 2007) and to antagonize STAT1 function (interferon signaling) by altering the nuclear import factors (Frieman et al., 2007). Indeed, interaction of SARS-CoV-2 Orf6 with proteins of the nuclear pore complex (Gordon et al., 2020) and its effect on IFN stimulated genes (ISG) (Prasad et al., 2020) have been reported recently. The interaction with the nuclear pore complex is evident from our data as well (Selinexor; Figure 6). SARS-CoV Nsp6 localizes to the endoplasmic reticulum, where it has been shown to interact with Nsp3 and Nsp4 to induce double-membrane vesicles (Angelini, Akhlaghpour, Neuman, & Buchmeier, 2013), and its SARS-CoV-2 equivalent has been predicted to interact with multiple ATPases of vesicle trafficking (Gordon et al., 2020). It might also interact with SIGMA1R, a receptor thought to regulate the endoplasmic reticulum stress response (Gordon et al., 2020). SARS-CoV-2 Orf7a protein has been predicted to interact with ribosomal transport proteins HEATR3 and MDN1 (Gordon et al., 2020). Previously, SARS-CoV Orf7a has been demonstrated to inhibit cellular translation

and induce apoptosis (Kopecky-Bromberg et al., 2006), in line with our viability data for SARS-CoV-2 Orf7a. The SARS-CoV protein was shown to interact with Bcl-X_L and other pro-survival proteins (Bcl-2, Bcl-2, Mcl-1, and A1), but not with pro-apoptotic proteins (Bax, Bak, Bad, and Bid) (Tan et al., 2007). The findings suggested Orf7a might trigger apoptosis by interfering directly with the pro-survival function of Bcl-X_L, indeed both proteins were shown to co-localize at the endoplasmic reticulum and mitochondria (Tan et al., 2007). Together, these findings indicate that even though the SARS-CoV-2 Orf6, Nsp6 and Orf7a proteins lead to similar viability defects and tissue damage, the underlying pathomechanisms are likely different.

SARS-CoV-2 Orf6 has been shown to act as an antagonist of IFN signaling (J. Y. Li et al., 2020; Miorin et al., 2020; Yuen et al., 2020) as well as to directly interact with the NUP98-RAE1 complex at the nuclear pore (Gordon et al., 2020; J. Li et al., 2020; Miorin et al., 2020). We similarly report SARS-CoV-2 Orf6 protein-protein interaction with many key members of the nuclear pore machinery, including nucleoporins and karyopherins (both importins and exportins) (Lee et al., this issue). Selinexor, an FDA-approved selective inhibitor of nuclear export (Syed, 2019), has been predicted to disrupt this interaction of SARS-CoV-2 Orf6 with the host nuclear pore complex (Gordon et al., 2020). We report it reduced SARS-CoV-2 Orf6 cytotoxic effects in a human in vitro culture model (Lee et al., this issue). Notably, the nuclear pore proteins in the Orf6 interaction network are extremely conserved between human and fly (Figure 1) (Lee et al., this issue), therefore we similarly treated the flies with this nuclear export inhibitor. Indeed, Selinexor treatment greatly attenuated the Orf6-induced muscle and trachea (lung) defects observed in fly (Figures 5 and 6). However, even though we found phenotypic overlap between Orf6, Orf7a and Nsp6 in our assays, Selinexor was unable to counteract Orf7a and Nsp6 effects, supporting the notion that the viral proteins act through different pathomechanisms. These findings further underpin our hypothesis that inhibition of viral entry/replication (the strategy of COVID-19 interventions like Remdesivir) might proof insufficient by itself as that approach might stop the virus in its tracks but does not remedy the multi-tissue effects of virus already present in the host. Therefore, we propose to use our Orf6 findings as a starting point to identify additional virus-host pathogenic interactions, then to develop drugs to target and disrupt these interactions. Therapeutic strategies, combining inhibition of virus entry/replication and pathogenic host interactions, would both stop SARS-CoV-2 spread and ameliorate the devastating progression of COVID-19 symptomatology.

In the current study, we have identified SARS-CoV-2 primary determinant pathogenic proteins (Orf6, Nsp6 and Orf7a). Capitalizing on the whole fly, enabled us to study the pathogenic effects of the individual viral proteins on muscle and trachea (lung). We expanded our understanding of the pathomechanism invoked by Orf6 and showed that Selinexor was able to attenuate Orf6 pathogenicity specifically *in vivo*. Together with the high conservation across the SARS-CoV-2 virus-host protein interaction network between human and fly, these data strongly support the fly as an effective model system for studying individual SARS-CoV-2 proteins.

Methods

Conservation SARS-CoV-2 and human host interactome in *Drosophila*

We used the DRSC Integrative Ortholog Prediction Tool (DIOPT) version 8 (Hu et al., 2011) for the identification of fly orthologs for the SARS-CoV-2 binding human proteins. DIOPT summarizes heterogeneous sources of conservation study tools and databases, providing integrative ortholog predictions, where score 0 indicates no orthologs and score 16 indicates all sources predicted the human-fly ortholog pair. Cytoscape version 3.8.0 (Shannon et al., 2003) was used to map the fly ortholog information (i.e. DIOPT scores) on to the SARS-CoV-2 human host interactome (Gordon et al., 2020).

Fly strains

All fly stocks were reared and kept on standard food at 25°C. The fly lines were obtained from the Bloomington Drosophila Stock Center (Indiana University, IN): w^{1118} (# BL-3605), *UAS-SARS-CoV-2 gene* overexpression (OE) strains, *Tubulin-Gal4/ TM3, Sb* (# BL-5138).

DNA cloning and generation of transgenic fly strains

The cDNA fragments were PCR-amplified from human codon-optimized SARS-CoV-2 genes (*Nsp1*, *Nsp2*, *Nsp3*, *Nsp6*, *Orf3a*, *Orf3b*, *Orf6*, *Orf7a*, *Orf7b*, *Orf8*, *Orf9b*, and *Orf10*) in pDONR207 vector (from Fritz Roth, through Addgene) or pLVX-EF1alpha-IRES-Puro vector (from Nevan Krogan, through Addgene), and assembled into the pUASTattB vector. The transgenes were introduced into a fixed chromosomal docking site by germ line transformation to generate *UAS-SARS-CoV-2-gene* overexpression (OE) transgenic flies.

Mortality at eclosion

In order to assay the effect of viral genes on viability, a balancer system was used. *UAS-SARS-CoV-2 gene* OE flies were crossed with a *Tub-Gal4/ TM3, Sb* line. Offspring either carry *UAS-SARS-CoV-2 gene OE/ TM3, Sb* which carry the balancer chromosome resulting in orange eye color, shortened (stubbly; Sb) hairs on the back and no transgene expression, or they carry *UAS-SARS-CoV-2 gene OE/ Tub-Gal4*, resulting in expression of the SARS-CoV-2 gene driven by *Tub-Gal4* and transgenic flies with the typical red eyes and long hair (Figure 2A). Embryo progeny were collected and allowed to develop under standard conditions. Mortality at eclosion (adult emergence from pupa stage) was based on the percentage of flies with SARS-CoV-2 gene expression (red, long) that failed to emerge as adults, relative to siblings that did not express the SARS-CoV-2 gene construct (orange, short). The result was presented as a Mortality Index calculated as: (long hair – short hair) / short hair X 100.

Adult survival assay

Following egg laying *Drosophila* larvae were kept at 25°C, standard conditions and an optimal temperature for *UAS*-transgene expression. Adult male flies were maintained in vials in groups of 20 or fewer. Number of life flies in each group was recorded every second day. *Drosophila* lifespan is typically 50-60 days for wild type flies. The assay was ended when no survivors were left for any of the transgenic lines. A 100 flies were assayed per genotype.

Climbing assay

Climbing male flies were monitored by analyzing their performance to climb 6 cm in a horizontal tube within 14 sec. A successful attempt was scored as 1, and failure to reach the top (6 cm line) as 0. Each fly was assessed five times to calculate the average climbing score. At least 30 flies per genotype were analyzed.

Drosophila wing observation

Wing position was observed using a ZEISS Stemi 305 Stereo Zoom microscope with 5:1 zoom. A total of 200 flies were counted (4 experimental replicates, 50 flies per group each time). Representative images were taken using a ZEISS SteREO Discovery.V12, modular stereo microscope with 12x zoom.

Drosophila indirect flight muscle imaging

Flies were dissected and fixed for 30 min in 4% paraformaldehyde in phosphate-buffered saline (1x PBS). Indirect flight muscle fibers from both wings were assayed. Alexa Fluor 647 phalloidin was obtained from Thermo Fisher. To label mitochondria, mouse anti-Atp5a antibody was used at 1:500, followed by Alexa Fluor 488-conjugated secondary antibodies. Confocal imaging of the *Drosophila* indirect fly muscle was performed using a ZEISS LSM900 confocal microscope with a 63× Plan-Apochromat 0.8 N.A. oil objective. For quantitative comparisons of fluorescence intensity, common settings were chosen to avoid oversaturation. ImageJ Software (version 1.52a) (Schneider, Rasband, & Eliceiri, 2012) was used to process images. Mitochondria were counted manually from the images, based on visual observation of rounded morphology separating individual segments (see Figure 6C, w^{1118} for example).

Imaging *Drosophila* tracheal branching

For tracheal observations, 3rd instar larvae were dissected as described previously (F. Chen, 2016). Six larvae were dissected for each group. Images of the tracheal branches for each were obtained using a using a ZEISS SteREO Discovery.V12, modular stereo microscope with 12x zoom. Tracheal branches in each segment were counted manually.

Selinexor treatment

Selinexor (Selleck, # KPT-330) was dissolved in dimethyl sulfoxide (DMSO; Sigma) and added to standard fly food at indicated doses (0.1, 0.2, and 0.5 μM). For untreated, control (0 μM), DMSO alone was added to the food. Flies were treated from first instar larval stage until the adult flies hatched.

Statistical analysis

Statistical tests were performed using PAST.exe software (http://folk.uio.no/ohammer/past/index.html) unless otherwise noted. Data were first tested for normality by using the Shapiro-Wilk test (a=0.05). Normally distributed data were analyzed either by Student's t-test (two groups) and Bonferroni

comparison to adjust the P value, or by a one-way analysis of variance followed by a Tukey-Kramer post-test for comparing multiple groups. Non-normal distributed data were analyzed by either a Mann–Whitney test (two groups) and Bonferroni comparison to adjust P value, or a Kruskal-Wallis H-test followed by a Dunn's test for comparisons between multiple groups. Statistical significance was defined as $P<0.05$.

Declarations

Ethics approval and consent to participate

Not applicable

Consent for publication

- The authors give our consent for publishing this work in Cell & Bioscience.

Availability of data and material

- All data and materials generated in this study are available publicly upon request.

Competing interests

- The authors declare no competing interest.

Funding

This work was supported, in part, by the University of Maryland Baltimore Institute for Clinical and Translational Research (UMB ICTR) COVID-19 Accelerated Translational Incubator Pilot (ATIP) grant to Dr. Han.

Authors' contributions

H. and J.Z. designed the study; J.Z. and J.L. carried out the experiments; J.Z., J.L., J.vdL. H. L., and Z.H. analyzed and interpreted the data; J.Z. and H.L. prepared the figures; J.vdL. and Z.H. drafted and revised the manuscript; the manuscript has been critically reviewed and the final version approved by all authors.

Acknowledgements

We thank Drs. Fritz Roth, Dr. Nevan Krogan and Addgene for the SARS-CoV-2 plasmids that containing most SARS-CoV-2 genes.

References

1. Angelini, M. M., Akhlaghpour, M., Neuman, B. W., & Buchmeier, M. J. (2013). Severe acute respiratory syndrome coronavirus nonstructural proteins 3, 4, and 6 induce double-membrane vesicles. *mBio,*

4(4). doi:10.1128/mBio.00524-13

2. Bao, L., Deng, W., Huang, B., Gao, H., Liu, J., Ren, L., . . . Qin, C. (2020). The pathogenicity of SARS-CoV-2 in hACE2 transgenic mice. *Nature*. doi:10.1038/s41586-020-2312-y
3. Battaglia, P. A., Zito, S., Macchini, A., & Gigliani, F. (2001). A Drosophila model of HIV-Tat-related pathogenicity. *J Cell Sci, 114*(Pt 15), 2787-2794. Retrieved from https://www.ncbi.nlm.nih.gov/pubmed/11683412
4. Chen, D., Wang, M., Zhou, S., & Zhou, Q. (2002). HIV-1 Tat targets microtubules to induce apoptosis, a process promoted by the pro-apoptotic Bcl-2 relative Bim. *EMBO J, 21*(24), 6801-6810. doi:10.1093/emboj/cdf683
5. Chen, F. (2016). Preparation and immunofluorescence staining of the trachea in Drosophila larvae and pupae. *Bio Protoc, 6*(9), e1797. doi:10.21769/BioProtoc.1797
6. Chen, Y., Guo, Y., Pan, Y., & Zhao, Z. J. (2020). Structure analysis of the receptor binding of 2019-nCoV. *Biochem Biophys Res Commun*. doi:10.1016/j.bbrc.2020.02.071
7. Dinnon, K. H., 3rd, Leist, S. R., Schafer, A., Edwards, C. E., Martinez, D. R., Montgomery, S. A., . . . Baric, R. S. (2020). A mouse-adapted model of SARS-CoV-2 to test COVID-19 countermeasures. *Nature*. doi:10.1038/s41586-020-2708-8
8. Fraser, C., Lythgoe, K., Leventhal, G. E., Shirreff, G., Hollingsworth, T. D., Alizon, S., & Bonhoeffer, S. (2014). Virulence and pathogenesis of HIV-1 infection: an evolutionary perspective. *Science, 343*(6177), 1243727. doi:10.1126/science.1243727
9. Frieman, M., Yount, B., Heise, M., Kopecky-Bromberg, S. A., Palese, P., & Baric, R. S. (2007). Severe acute respiratory syndrome coronavirus ORF6 antagonizes STAT1 function by sequestering nuclear import factors on the rough endoplasmic reticulum/Golgi membrane. *J Virol, 81*(18), 9812-9824. doi:10.1128/JVI.01012-07
10. Gordon, D. E., Jang, G. M., Bouhaddou, M., Xu, J., Obernier, K., White, K. M., . . . Krogan, N. J. (2020). A SARS-CoV-2 protein interaction map reveals targets for drug repurposing. *Nature*. doi:10.1038/s41586-020-2286-9
11. Harsh, S., Fu, Y., Kenney, E., Han, Z., & Eleftherianos, I. (2020). Zika virus non-structural protein NS4A restricts eye growth in Drosophila through regulation of JAK/STAT signaling. *Dis Model Mech, 13*(4). doi:10.1242/dmm.040816
12. Hassan, A. O., Case, J. B., Winkler, E. S., Thackray, L. B., Kafai, N. M., Bailey, A. L., . . . Diamond, M. S. (2020). A SARS-CoV-2 Infection Model in Mice Demonstrates Protection by Neutralizing Antibodies. *Cell, 182*(3), 744-753 e744. doi:10.1016/j.cell.2020.06.011
13. Hu, Y., Flockhart, I., Vinayagam, A., Bergwitz, C., Berger, B., Perrimon, N., & Mohr, S. E. (2011). An integrative approach to ortholog prediction for disease-focused and other functional studies. *BMC Bioinformatics, 12*, 357. doi:10.1186/1471-2105-12-357
14. Hughes, T. T., Allen, A. L., Bardin, J. E., Christian, M. N., Daimon, K., Dozier, K. D., . . . Ahlander, J. (2012). Drosophila as a genetic model for studying pathogenic human viruses. *Virology, 423*(1), 1-5. doi:10.1016/j.virol.2011.11.016

15. Israelow, B., Song, E., Mao, T., Lu, P., Meir, A., Liu, F., . . . Iwasaki, A. (2020). Mouse model of SARS-CoV-2 reveals inflammatory role of type I interferon signaling. *J Exp Med, 217*(12). doi:10.1084/jem.20201241
16. Kashyap, T., Argueta, C., Aboukameel, A., Unger, T. J., Klebanov, B., Mohammad, R. M., . . . Landesman, Y. (2016). Selinexor, a Selective Inhibitor of Nuclear Export (SINE) compound, acts through NF-kB deactivation and combines with proteasome inhibitors to synergistically induce tumor cell death. *Oncotarget, 7*(48), 78883-78895. doi:10.18632/oncotarget.12428
17. Khan, S., Fielding, B. C., Tan, T. H., Chou, C. F., Shen, S., Lim, S. G., . . . Tan, Y. J. (2006). Over-expression of severe acute respiratory syndrome coronavirus 3b protein induces both apoptosis and necrosis in Vero E6 cells. *Virus Res, 122*(1-2), 20-27. doi:10.1016/j.virusres.2006.06.005
18. Kopecky-Bromberg, S. A., Martinez-Sobrido, L., Frieman, M., Baric, R. A., & Palese, P. (2007). Severe acute respiratory syndrome coronavirus open reading frame (ORF) 3b, ORF 6, and nucleocapsid proteins function as interferon antagonists. *J Virol, 81*(2), 548-557. doi:10.1128/JVI.01782-06
19. Kopecky-Bromberg, S. A., Martinez-Sobrido, L., & Palese, P. (2006). 7a protein of severe acute respiratory syndrome coronavirus inhibits cellular protein synthesis and activates p38 mitogen-activated protein kinase. *J Virol, 80*(2), 785-793. doi:10.1128/JVI.80.2.785-793.2006
20. Law, P. T. W., Wong, C. H., Au, T. C. C., Chuck, C. P., Kong, S. K., Chan, P. K. S., . . . Tsui, S. K. W. (2005). The 3a protein of severe acute respiratory syndrome-associated coronavirus induces apoptosis in Vero E6 cells. *J Gen Virol, 86*(Pt 7), 1921-1930. doi:10.1099/vir.0.80813-0
21. Lee, S. B., Park, J., Jung, J. U., & Chung, J. (2005). Nef induces apoptosis by activating JNK signaling pathway and inhibits NF-kappaB-dependent immune responses in Drosophila. *J Cell Sci, 118*(Pt 9), 1851-1859. doi:10.1242/jcs.02312
22. Li, J., Guo, M., Tian, X., Wang, X., Yang, X., Wu, P., . . . Liang, Q. (2020). Virus-Host Interactome and Proteomic Survey Reveal Potential Virulence Factors Influencing SARS-CoV-2 Pathogenesis. *Med (N Y)*. doi:10.1016/j.medj.2020.07.002
23. Li, J. Y., Liao, C. H., Wang, Q., Tan, Y. J., Luo, R., Qiu, Y., & Ge, X. Y. (2020). The ORF6, ORF8 and nucleocapsid proteins of SARS-CoV-2 inhibit type I interferon signaling pathway. *Virus Res, 286*, 198074. doi:10.1016/j.virusres.2020.198074
24. Link, N., Chung, H., Jolly, A., Withers, M., Tepe, B., Arenkiel, B. R., . . . Bellen, H. J. (2019). Mutations in ANKLE2, a ZIKA Virus Target, Disrupt an Asymmetric Cell Division Pathway in Drosophila Neuroblasts to Cause Microcephaly. *Dev Cell, 51*(6), 713-729 e716. doi:10.1016/j.devcel.2019.10.009
25. Liu, Y., Gordesky-Gold, B., Leney-Greene, M., Weinbren, N. L., Tudor, M., & Cherry, S. (2018). Inflammation-Induced, STING-Dependent Autophagy Restricts Zika Virus Infection in the Drosophila Brain. *Cell Host Microbe, 24*(1), 57-68 e53. doi:10.1016/j.chom.2018.05.022
26. Miorin, L., Kehrer, T., Sanchez-Aparicio, M. T., Zhang, K., Cohen, P., Patel, R. S., . . . Garcia-Sastre, A. (2020). SARS-CoV-2 Orf6 hijacks Nup98 to block STAT nuclear import and antagonize interferon signaling. *Proc Natl Acad Sci U S A, 117*(45), 28344-28354. doi:10.1073/pnas.2016650117

27. Prasad, K., Khatoon, F., Rashid, S., Ali, N., AlAsmari, A. F., Ahmed, M. Z., . . . Kumar, V. (2020). Targeting hub genes and pathways of innate immune response in COVID-19: A network biology perspective. *Int J Biol Macromol, 163*, 1-8. doi:10.1016/j.ijbiomac.2020.06.228

28. Rockx, B., Kuiken, T., Herfst, S., Bestebroer, T., Lamers, M. M., Oude Munnink, B. B., . . . Haagmans, B. L. (2020). Comparative pathogenesis of COVID-19, MERS, and SARS in a nonhuman primate model. *Science, 368*(6494), 1012-1015. doi:10.1126/science.abb7314

29. Schaecher, S. R., Touchette, E., Schriewer, J., Buller, R. M., & Pekosz, A. (2007). Severe acute respiratory syndrome coronavirus gene 7 products contribute to virus-induced apoptosis. *J Virol, 81*(20), 11054-11068. doi:10.1128/JVI.01266-07

30. Schneider, C. A., Rasband, W. S., & Eliceiri, K. W. (2012). NIH Image to ImageJ: 25 years of image analysis. *Nat Methods, 9*(7), 671-675. doi:10.1038/nmeth.2089

31. Shannon, P., Markiel, A., Ozier, O., Baliga, N. S., Wang, J. T., Ramage, D., . . . Ideker, T. (2003). Cytoscape: a software environment for integrated models of biomolecular interaction networks. *Genome Res, 13*(11), 2498-2504. doi:10.1101/gr.1239303

32. Syed, Y. Y. (2019). Selinexor: First Global Approval. *Drugs, 79*(13), 1485-1494. doi:10.1007/s40265-019-01188-9

33. Takayama, K. (2020). In Vitro and Animal Models for SARS-CoV-2 research. *Trends Pharmacol Sci, 41*(8), 513-517. doi:10.1016/j.tips.2020.05.005

34. Tan, Y. X., Tan, T. H., Lee, M. J., Tham, P. Y., Gunalan, V., Druce, J., . . . Tan, Y. J. (2007). Induction of apoptosis by the severe acute respiratory syndrome coronavirus 7a protein is dependent on its interaction with the Bcl-XL protein. *J Virol, 81*(12), 6346-6355. doi:10.1128/JVI.00090-07

35. UniProt, C. (2019). UniProt: a worldwide hub of protein knowledge. *Nucleic Acids Res, 47*(D1), D506-D515. doi:10.1093/nar/gky1049

36. Wang, A., Thurmond, S., Islas, L., Hui, K., & Hai, R. (2017). Zika virus genome biology and molecular pathogenesis. *Emerg Microbes Infect, 6*(3), e13. doi:10.1038/emi.2016.141

37. Yoshimoto, F. K. (2020). The Proteins of Severe Acute Respiratory Syndrome Coronavirus-2 (SARS CoV-2 or n-COV19), the Cause of COVID-19. *Protein J, 39*(3), 198-216. doi:10.1007/s10930-020-09901-4

38. Yu, P., Qi, F., Xu, Y., Li, F., Liu, P., Liu, J., . . . Qin, C. (2020). Age-related rhesus macaque models of COVID-19. *Animal Model Exp Med, 3*(1), 93-97. doi:10.1002/ame2.12108

39. Yuan, X., Shan, Y., Zhao, Z., Chen, J., & Cong, Y. (2005). G0/G1 arrest and apoptosis induced by SARS-CoV 3b protein in transfected cells. *Virol J, 2*, 66. doi:10.1186/1743-422X-2-66

40. Yuen, C. K., Lam, J. Y., Wong, W. M., Mak, L. F., Wang, X., Chu, H., . . . Kok, K. H. (2020). SARS-CoV-2 nsp13, nsp14, nsp15 and orf6 function as potent interferon antagonists. *Emerg Microbes Infect, 9*(1), 1418-1428. doi:10.1080/22221751.2020.1780953

Figures

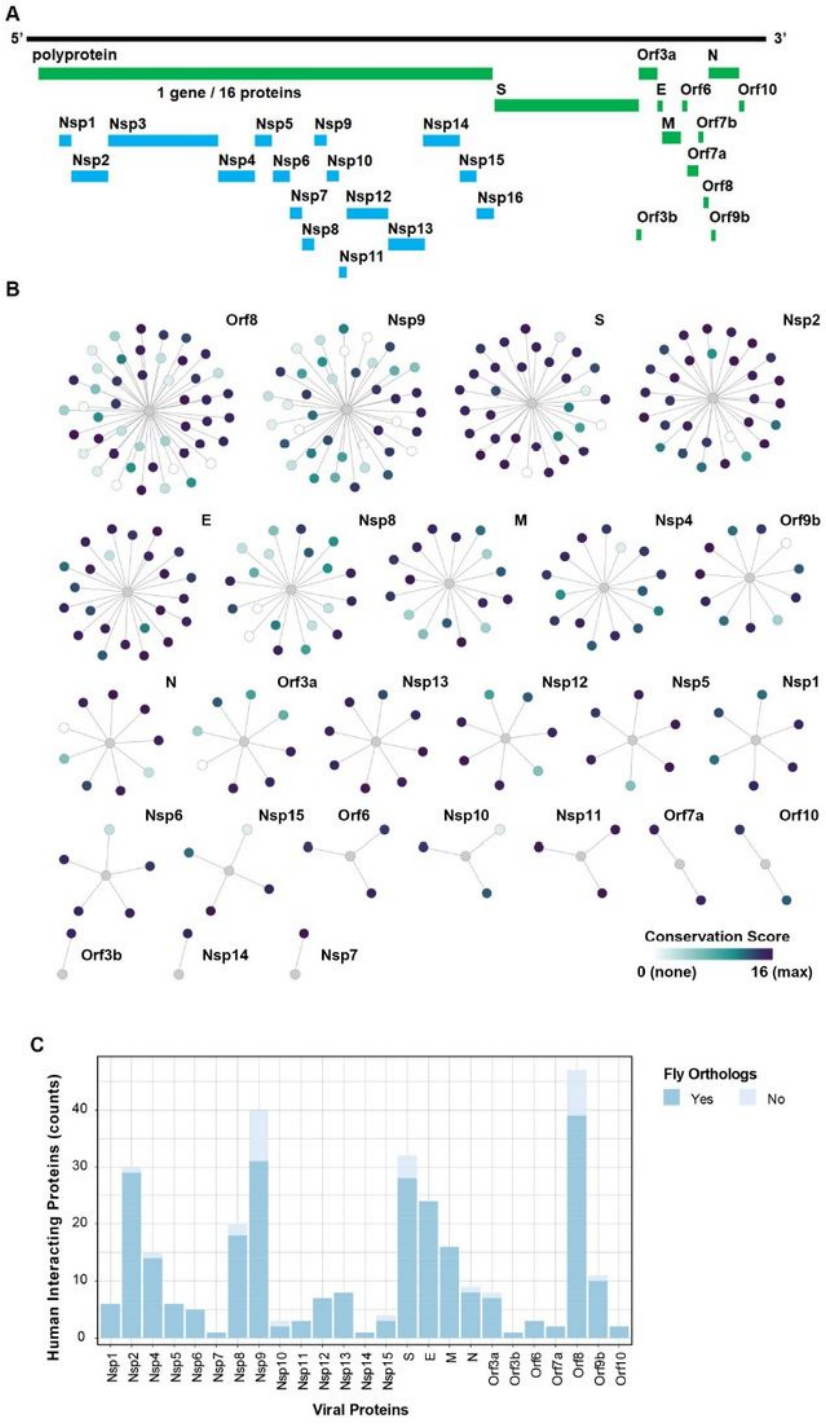

Figure 1

SARS-CoV-2 human protein-protein host interactome is conserved in Drosophila. (A) Schematic representation of SARS-CoV-2 genome. (B) Graphic display of the conservation of the SARS-CoV-2 and human host interactome in Drosophila. The graphs summarize the high-confidence interactions between SARS-CoV-2 proteins (bait, gray node) and human proteins (prey) described in Gordon et al. (Gordon et al., 2020). Human interacting proteins are colored based on their conservation score (i.e. DIOPT score (Hu et

al., 2011)) for the best matching fly ortholog. (C) Bargraph summarizes the ortholog information displayed in (B). SARS-CoV-2 interacting human proteins that have fly orthologs defined or predicted by more than one source (i.e. DIOPT score >= 2) have been included.

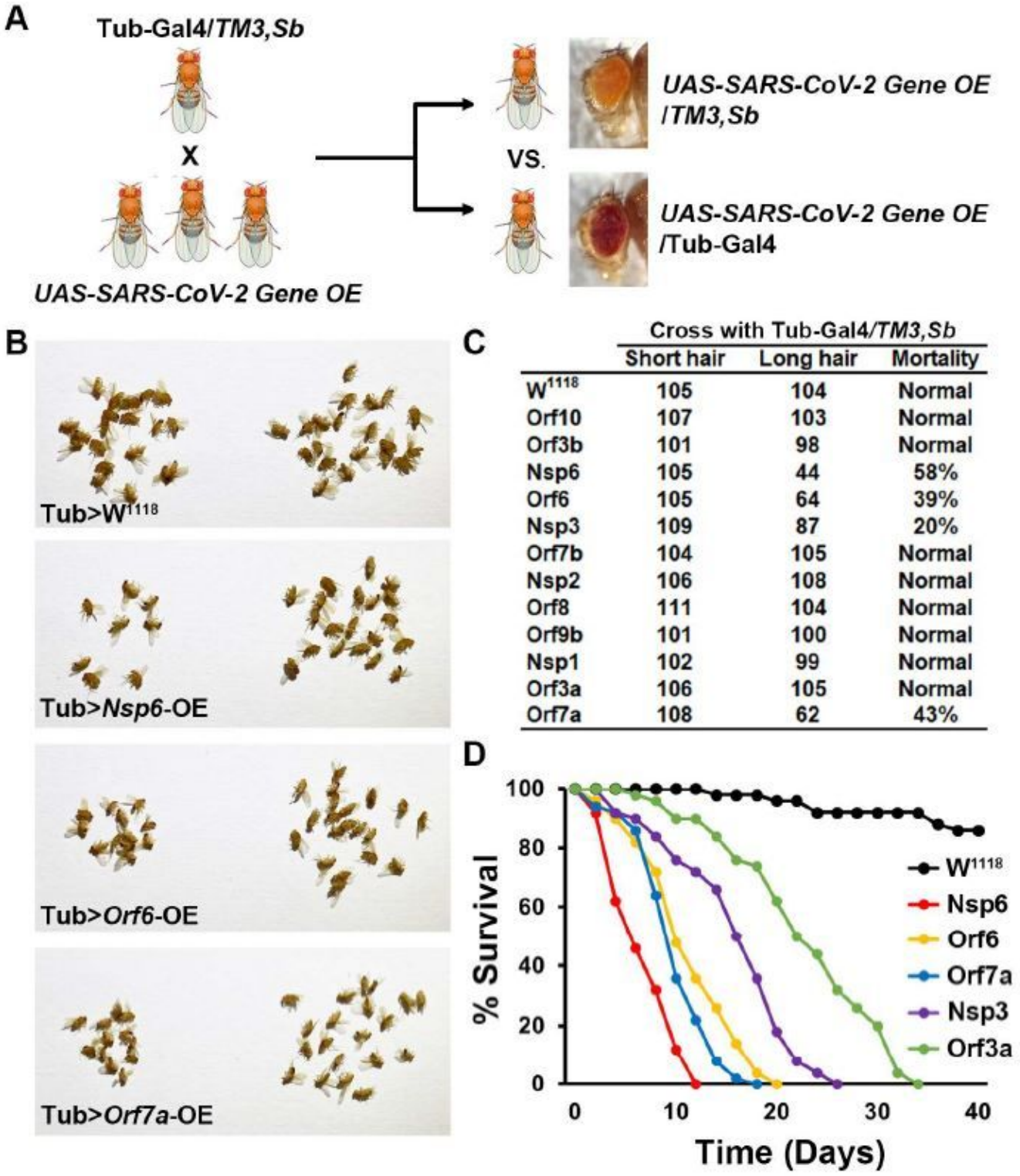

Figure 2

SARS-CoV-2 Nsp6, Orf6 and Orf7a transgene expression causes developmental lethality. (A) Schematic representation of genetic screen to identify individual SARS-CoV-2 genes with pathogenic effect. (B)

Images of adult progeny emerging from pupa stage from cross in (A), distinguished by carrying the balancer (TM3, Sb; orange eyes and short hair on back; no viral transgene expression) or with expression of the SARS-CoV-2 gene driven by the ubiquitous Tubulin (Tub) enhancer (red eyes and long hair). w1118 is a wild type control. (C) Quantification of mortality rate prior to eclosion for the individually expressed SARS-CoV-2 genes from the cross in (A). Mortality calculated as: (long hair – short hair) / short hair X 100. (D) Graph displaying lifespan data for adult flies carrying SARS-CoV-2 Nsp6, Orf6, Orf7a, Nsp3 or Orf3a transgenes. w1118 is a wild type control. N=100 flies per group. Abbreviations: E, envelope protein; M, membrane protein; N, nucleocapsid protein; Nsp, non-structural protein; OE, overexpression; Orf, accessory protein; S, spike protein; Sb, stubble TM3, chromosome 3.

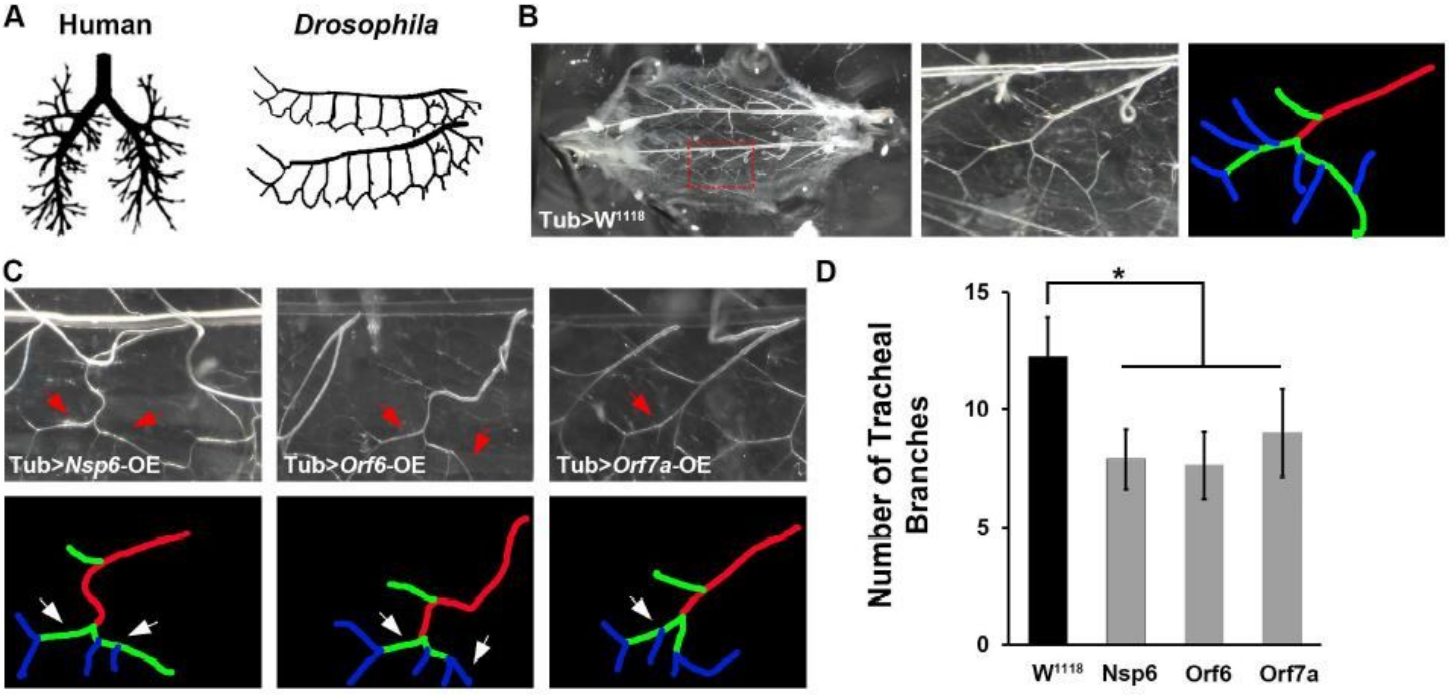

Figure 3

SARS-CoV2 Nsp6, Orf6 and Orf7a transgene expression leads to reduced tracheal branching in Drosophila. (A) Graphic representation of branching in human lung (left) and Drosophila trachea (right). (B) Typical tracheal branches in wild type larva (w1118). Left panel, overview of complete Drosophila trachea system. Red box denotes area shown at higher magnification in middle panel, as well as area covered in images shown in C. Right panel, labeling of tracheal branches: red, central branch; green, class I terminal branch; and, blue, class II terminal branch. (C) Representative images of tracheal branches (taken at location equivalent to red box in B) in SARS-CoV-2 Nsp6, Orf6 or Orf7a overexpression (OE) transgenic flies. Arrow indicates a missing class II terminal branch based on wild type (w1118 shown in B). Tracheal branches are labeled to indicate the central branch (red), class I terminal branch (green), and class II terminal branch (blue). (D) Quantification of tracheal branch numbers in one segment. N=6 larvae per group. Results are presented as mean ±SD. Statistical significance (*) is defined as $P<0.05$.

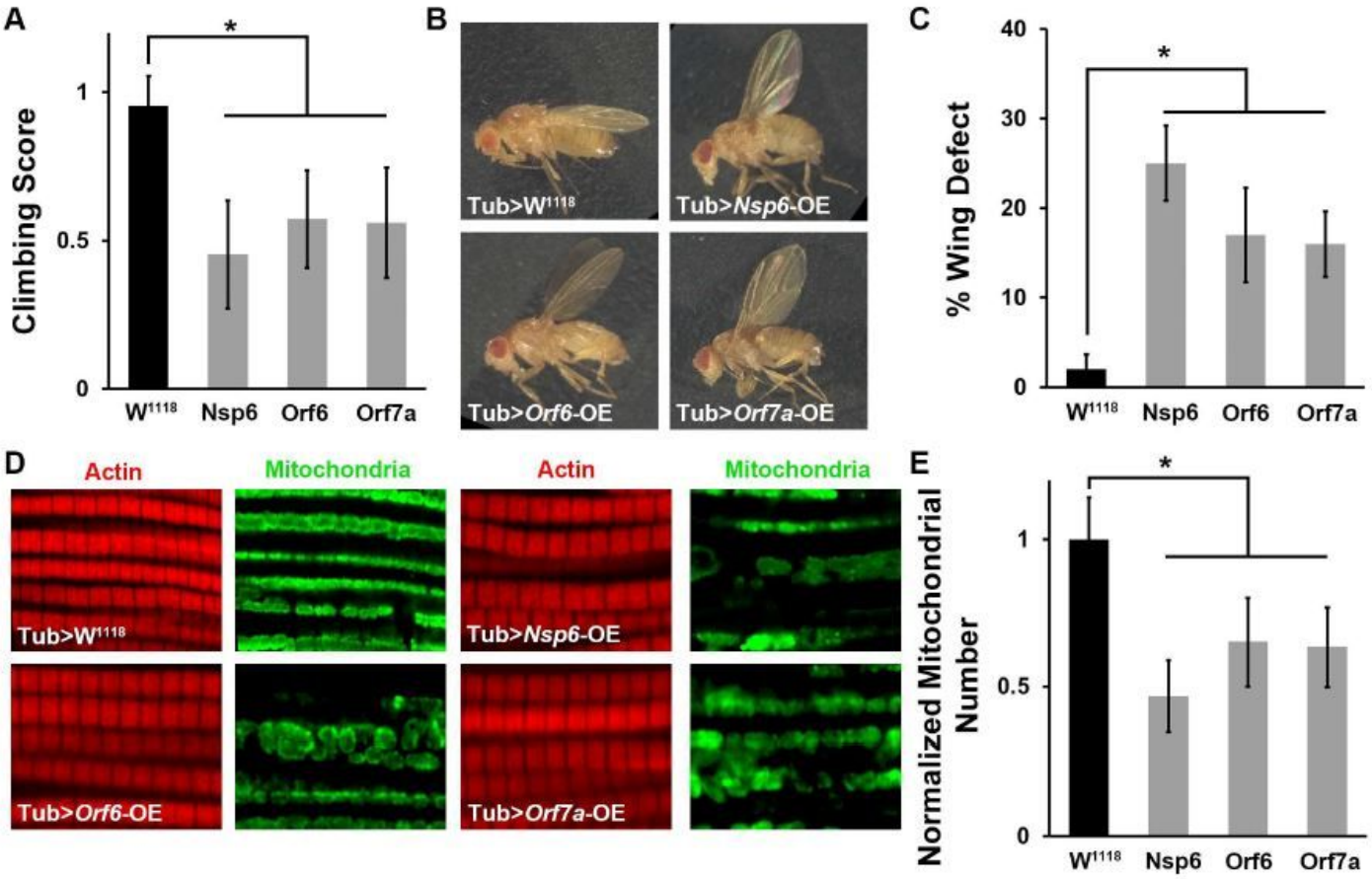

Figure 4

SARS-CoV-2 Nsp6, Orf6 and Orf7a transgene expression in Drosophila results in locomotion defect and reduced mitochondria. (A) Quantification of climbing ability in SARS-CoV-2 Nsp6, Orf6 and Orf7a transgenic flies. N=30 flies per group. (B) Representative images of typical (wild type, w1118) and “held-up” wing phenotype in SARS-CoV-2 Nsp6, Orf6 and Orf7a expression flies. (C) Quantification of flies with “held-up” wing phenotype (i.e. % Wing Defect). Four replicates, each replicate N=50 flies per group. (D) Representative images of indirect flight muscle (labeled with Phalloidin, red) and mitochondria (labeled with ATP5A, green) morphology in SARS-CoV-2 Nsp6, Orf6 and Orf7a flies. (E) Quantification of the number of mitochondria in the fly indirect flight muscle of both wings, normalized based on wild type (w1118) counts. N=10 flies per group. The results are presented as mean ±SD. Statistical significance (*) is defined as $P<0.05$.

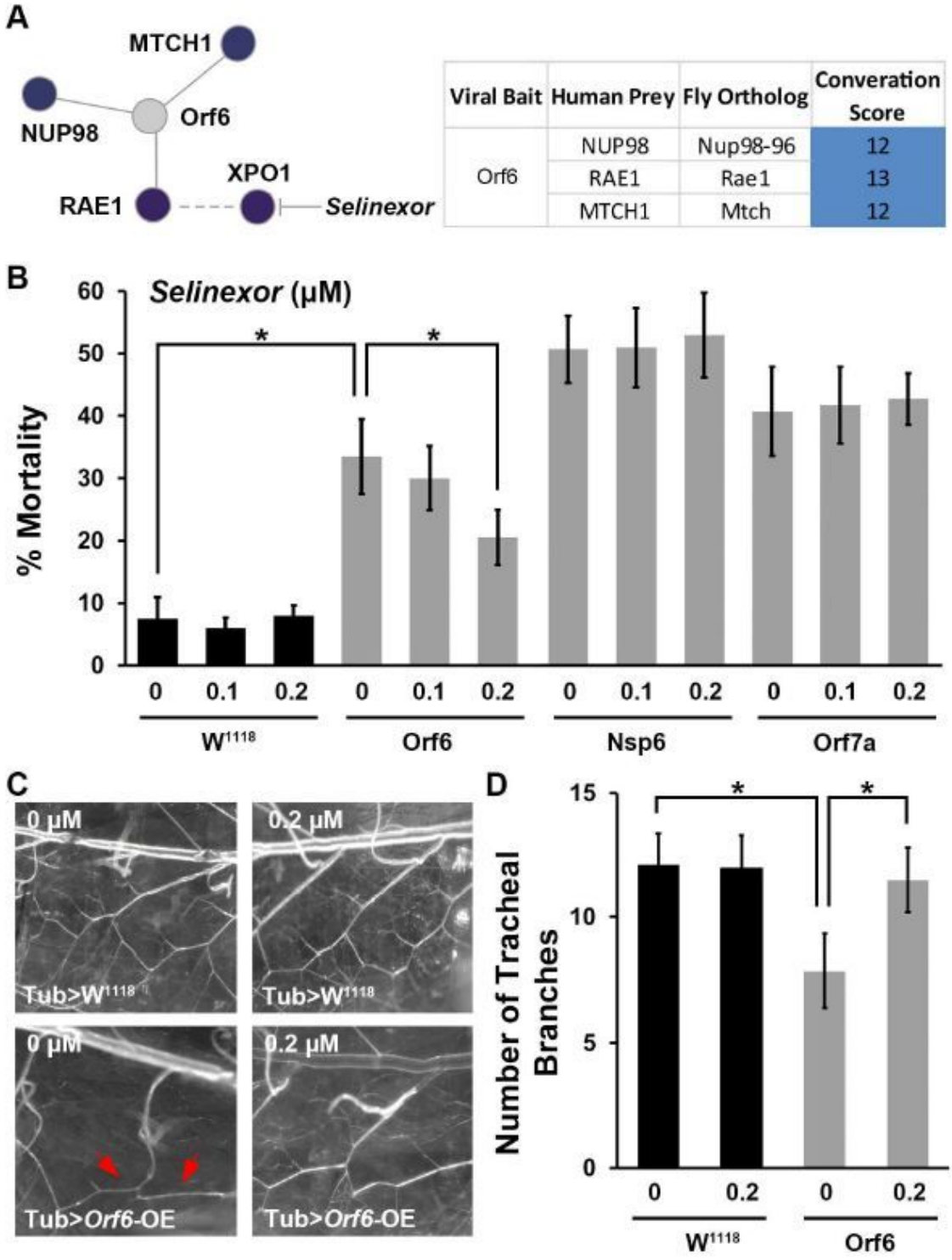

Viral Bait	Human Prey	Fly Ortholog	Converation Score
Orf6	NUP98	Nup98-96	12
	RAE1	Rae1	13
	MTCH1	Mtch	12

Figure 5

Selinexor attenuates fly developmental lethality and reduction in tracheal branching induced by SARS-CoV-2 Orf6 transgene expression. (A) Graphic presentation of conservation SARS-CoV-2 Orf6 interaction with human host proteins in Drosophila. Graph summarized the high-confidence interactions between SARS-CoV-2 Orf6 protein (bait, grey node) and human proteins (prey) described in Gordon et al. (Gordon et al., 2020). Human interacting proteins are colored based on their conservation score (i.e. DIOPT score

(Hu et al., 2011)) of the best matching fly ortholog. Numeric conservation scores human-fly proteins provided in table. (B) Quantification of mortality rate prior to eclosion for wild type (w1118) or SARS-CoV-2 Orf6, Nsp6 or Orf7a transgenic flies (overexpression (OE) driven by ubiquitous enhancer Tubulin (Tub)) following treatment with different doses of Selinexor. Mortality calculated as: (long hair – short hair) / short hair X 100. Four replicates, each replicate N=50 flies per group. (C) Representative images of tracheal branches (taken at location equivalent to red box in Figure 3B) in wild type (w1118) and SARS-CoV-2 Orf6 overexpression (OE) transgenic flies, with (0.2 μM) or without (0 μM) Selinexor treatment. Arrow indicates a missing class II terminal branch based on typical wild type pattern. (D) Quantification of tracheal branch numbers in one segment for observations in (C). N=6 larvae per group. Results are presented as mean ±SD. Statistical significance (*) is defined as $P<0.05$.

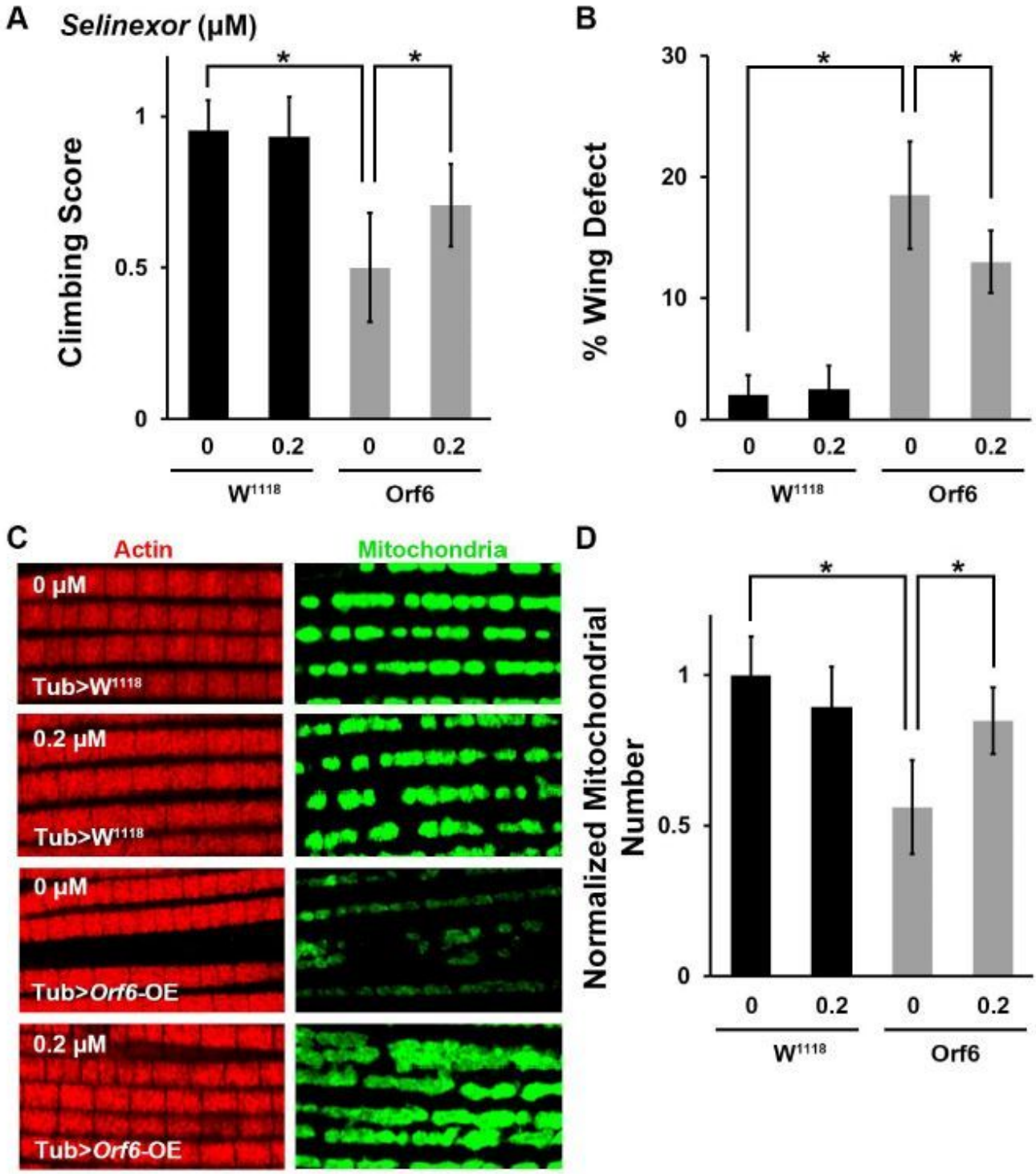

Figure 6

Selinexor attenuates locomotion defect and reduced mitochondria caused by SARS-CoV-2 Orf6 transgene expression in flies. Comparative assays of phenotypes in wild type (w1118) and SARS-CoV-2 Orf6 transgenic (overexpression (OE) driven by ubiquitous enhancer Tubulin (Tub)) flies following treatment with Selinexor (0.2 μM). (A) Quantification of climbing ability. N=30 flies per group. (B) Quantification of flies with “held-up” wing phenotype (i.e. % Wing Defect). Four replicates, each replicate N=50 flies per

group. (C) Representative images of indirect flight muscle (labeled with Phalloidin, red) and mitochondria (labeled with ATP5A, green) morphology. (D) Quantification of the number of mitochondria in the fly indirect flight muscle, normalized based on wild type (w1118) counts. N=10 flies per group. Results are presented as mean ±SD. Statistical significance (*) is defined as $P<0.05$.

Supplementary Files

This is a list of supplementary files associated with this preprint. Click to download.

- ZhuetalSupplTableS1formattedJL09162020.pdf